

Doping dependence of the Nernst effect in $\text{Eu}(\text{Fe}_{1-x}\text{Co}_x)_2\text{As}_2$ - departure from Dirac fermions physics

Marcin Matusiak¹, Zbigniew Bukowski², and Janusz Karpinski²

1. Institute of Low Temperature and Structural Research,

Polish Academy of Sciences, P.O. Box 1410, 50-950 Wroclaw, Poland and

2. Laboratory for Solid State Physics, ETH Zurich, 8093 Zurich, Switzerland

(Dated: March 10, 2022)

We report a systematic study of the transport properties in the series of $\text{Eu}(\text{Fe}_{1-x}\text{Co}_x)_2\text{As}_2$ single crystals with $x = 0, 0.15, 0.20$ and 0.30 . Spin-density-wave order is observed in the undoped and the least doped samples ($x = 0, 0.15$), while for $x = 0.15$ and 0.20 $\text{Eu}(\text{Fe}_{1-x}\text{Co}_x)_2\text{As}_2$ becomes a superconductor. We found the properties of the parent EuFe_2As_2 compound well described by the Dirac fermions model, whereas cobalt doping caused an evolution of the system toward a regular metallic state. The antiferromagnetic ordering of the Eu^{2+} ions at $T_N \approx 20$ K has only minor influence on the measured quantities.

PACS numbers: 72.15.Jf, 74.25.F-, 74.70.Xa

There is a substantial difference between the antiferromagnetic ground states of the parent compounds of copper- and iron-based superconductors. While the first is the Mott insulator [1], the spin-density-wave (SDW) state in the second is always metallic [2]. Since the Cooper pairing interaction is probably magnetic in both families, understanding of the evolution of the system from magnetism to superconductivity (SC) can be a crucial step towards revealing the mechanism responsible for superconductivity. In this letter we investigate the $\text{Eu}(\text{Fe}_{1-x}\text{Co}_x)_2\text{As}_2$ series of iron-pnictide single crystals and report Nernst coefficient (ν) data together with complementary studies of the thermoelectric power (S), Hall coefficient (R_H) and resistivity (ρ). The dominating influence of Dirac fermions on the transport properties seen in the parent EuFe_2As_2 compound vanishes with cobalt doping and our most highly doped $\text{Eu}(\text{Fe}_{0.7}\text{Co}_{0.3})_2\text{As}_2$ shows regular metallic behavior. In the least doped $\text{Eu}(\text{Fe}_{0.85}\text{Co}_{0.15})_2\text{As}_2$ we observe both superconductivity and spin-density-wave order. However, the influence of SDW on ν changes radically in comparison with the undoped EuFe_2As_2 . This may indicate that Dirac fermions cannot survive in the sample that shows both SDW and SC.

Single crystals of $\text{Eu}(\text{Fe}_{1-x}\text{Co}_x)_2\text{As}_2$ were grown out of Sn flux. The constituent elements were loaded into alumina crucibles and placed in quartz ampoules sealed under pressure of 0.3 bar of Ar. The ampoules were heated to 1050°C and kept at that temperature for 10 h to ensure complete dissolving of all components in molten Sn. Next, the ampoules were slowly (2-3°C/h) cooled down to 600°C, then liquid Sn-flux was decanted and remaining Sn was etched away from crystals with hydrochloric acid. To cover all possible SDW/SC configurations shown in Table 1, we selected four compositions for further studies: $x=0$ (denoted as Co-0), $x=0.15$ (Co-15), $x=0.20$ (Co-20), and $x=0.30$ (Co-30). The cobalt content was determined by the energy dispersive x-ray (EDX) analysis,

TABLE I: The lattice parameters and the influence of cobalt content on the presence/absence of the SDW and SC order in $\text{Eu}(\text{Fe}_{1-x}\text{Co}_x)_2\text{As}_2$.

x	a (Å)	c (Å)	SDW, T_{SDW} (K)	SC, T_c (K)
0	3.898(1)	12.11(1)	present, 191 K	absent, -
0.15	3.904(1)	12.08(1)	present, 131 K	present, 7.7 K
0.20	3.911(1)	12.06(1)	absent, -	present, 5.2 K
0.30	3.912(1)	12.03(1)	absent, -	absent, -

which gave us values that were larger than the nominal and typical values from other studies [7–9]. We ascribe this to uncertainties arising from partial overlap of the main Eu, Fe and Co peaks in energy dispersive x-ray spectra. Therefore, the presented here absolute values of x should be treated only as estimates. The phase purity was checked by powder X-ray diffraction (XRD). All the observed diffraction lines on the XRD pattern could be indexed on the basis of the tetragonal ThCr_2Si_2 -type structure (space group $I4/mmm$). Both a and c lattice parameters show the systematic, but weak evolution with x (see Table 1).

The methods of measurements of the electrical resistivity, Hall coefficient, thermoelectric power, and Nernst coefficient were the same as described in Ref. [3] with one important difference. In Ref. [3] we used the old sign convention, according to which the vortex Nernst signal is negative, whereas in the present paper we use a recently more popular convention [4]. This results in opposite Nernst coefficients of $\text{CaFe}_{2-x}\text{Co}_x\text{As}_2$ [3] and $\text{Eu}(\text{Fe}_{1-x}\text{Co}_x)_2\text{As}_2$, despite the fact that Nernst signals in both materials have the same sign.

The temperature dependences of the electrical resistivity shown in Fig.1 reveal the emergence of the SDW state, which is accompanied by the structural transition [5], at $T_{SDW} = 191$ K for Co-0 and $T_{SDW} = 131$ K for Co-15.

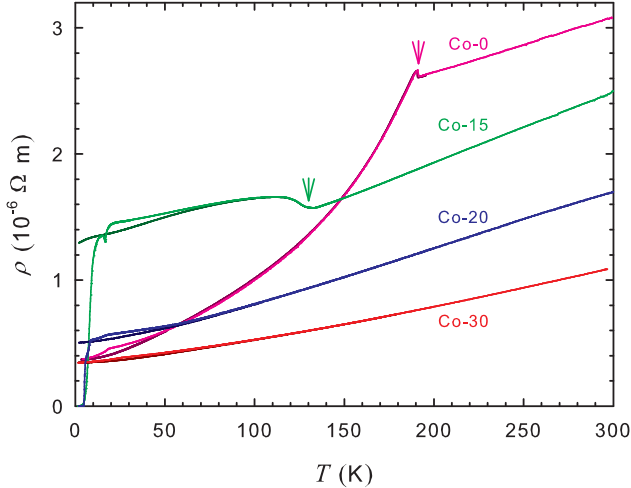


FIG. 1: (Color online) The temperature dependences of the resistivities of the $\text{Eu}(\text{Fe}_{1-x}\text{Co}_x)_2\text{As}_2$ series. At low temperatures the lines deviating upward are measured at $B = 0$ T, while their featureless counterparts are measured in field of 12.5 or 13 T. Arrows indicate the onset of the SDW order in Co-0 and Co-15.

Additionally, we observe the superconducting transition in Co-15 and Co-20 at $T_c = 7.7$ K and $T_c = 5.2$ K, respectively (T_c is defined as the maximum in $d\rho/dT$). At low magnetic field ($B \lesssim 0.5$ T) the onset of the superconducting transition in the Co-15 crystal is notably above T_c , but below 17 K the resistivity temporarily goes back to its normal value as superconductivity is destroyed by the competing antiferromagnetic order of the Eu^{2+} ions [6]. Analogous reentrant behavior was already reported for $\text{Eu}(\text{Fe}_{1-x}\text{Co}_x)_2\text{As}_2$ [7, 9], $\text{EuFe}_2(\text{As}_{1-x}\text{P}_x)_2$ [10, 11], and the undoped EuFe_2As_2 under pressure [12]. The Eu^{2+} ordering is visible in the all studied samples as a small and broad peak in $\rho(T)$ around $T = 20$ K. This peak is completely eradicated by magnetic field of the order of 10 T. This happens irrespectively of the B vector orientation (for Co-20 B is parallel to the c crystallographic axis, for all other samples B is perpendicular to c). Such a magnetic field is also sufficient to completely suppress the superconducting transition, or at least, to shift T_c below $T \approx 2$ K. Fig. 2 presents the temperature and doping dependences of the Hall coefficient ($B \approx 13$ T) - panel (a), thermoelectric power ($B = 0$ T) - panel (b), and the Nernst coefficient ($B \approx 13$ T) - panel (c) for the $\text{Eu}(\text{Fe}_{1-x}\text{Co}_x)_2\text{As}_2$ series. The high temperature properties of all measured quantities systematically evolve with increasing x towards the characteristics of a regular metal represented by Co-30, the crystal with the highest doping. For this sample R_H is small and weakly temperature dependent, S is nearly linear with T , and ν becomes very small ($|\nu| < 5$ $\text{nV K}^{-1} \text{T}^{-1}$) as expected in the case of the satisfied Sondheimer cancellation [13]. The Nernst coef-

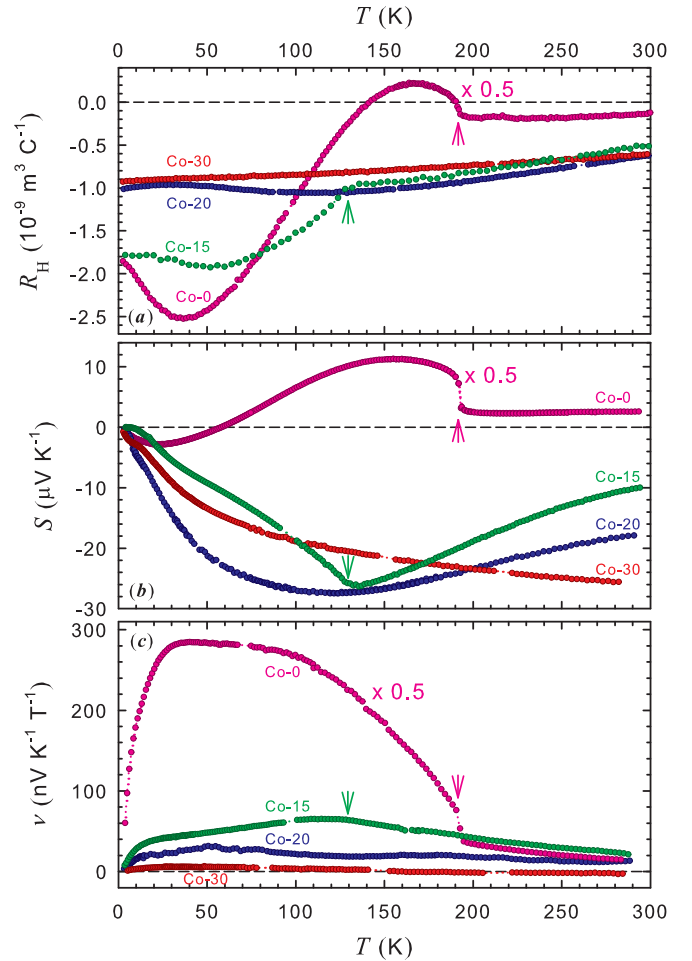


FIG. 2: (Color online) The temperature dependences of the Hall coefficient (panel a), thermoelectric power (panel b) and Nernst coefficient (panel c) for the $\text{Eu}(\text{Fe}_{1-x}\text{Co}_x)_2\text{As}_2$ series. All coefficients for Co-0 are divided by 2. Arrows indicate T_{SDW} for Co-0 and Co-15.

TABLE II: Summary of results at the low temperature limit.

x	μ_H (T^{-1})	ν/T ($\text{nV K}^{-2} \text{T}^{-1}$)	T_F (K)
0	-0.0098	34	80
0.15	-0.0014	2.3	170
0.20	-0.002	1.3	440
0.30	-0.0027	0.3	2500

ficient at zero temperature can be related to the Fermi temperature (T_F) and Hall mobility ($\mu_H \equiv \frac{\sigma_{xy}}{B\sigma_{xx}} = \frac{R_H}{\rho}$) through the equation: $\nu = \frac{\pi 2k_B}{3e} \frac{T\mu_H}{T_F}$ [4], where k_B is the Boltzmann constant and e is the elementary charge. As seen in Fig. 3, low temperature values of ν/T saturate for all samples and can be used to estimate the Fermi energy. The approximative ($\text{Eu}(\text{Fe}_{1-x}\text{Co}_x)_2\text{As}_2$ is a multi-band system) values of T_F together with ν/T and μ_H are collected in Tab. 2.

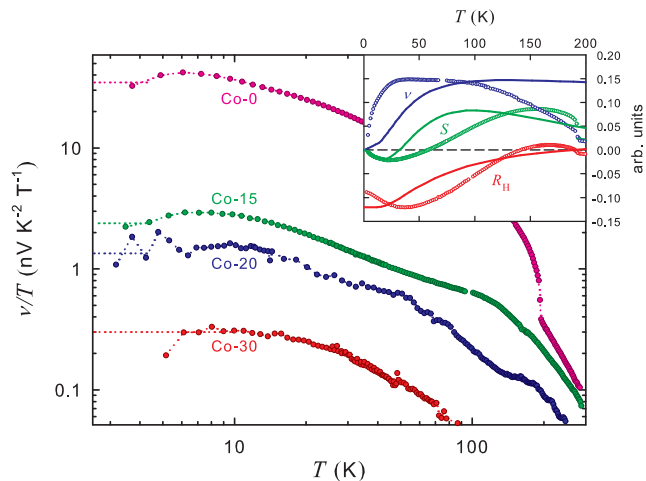


FIG. 3: (Color online) The magnitude of the Nernst coefficient divided by temperature for the $\text{Eu}(\text{Fe}_{1-x}\text{Co}_x)_2\text{As}_2$ series plotted versus temperature on a logarithmic scale. Dotted lines are guides for the eye. Inset shows temperature dependences of transport coefficients for Co-0 compared with theoretical results from Ref. [15].

Intriguingly, the crystal with the lowest Fermi energy ($\varepsilon_F \approx 7$ meV) has at low temperatures clearly the highest μ_H , and such a significantly enhanced mobility can be a manifestation of limited scattering of the Dirac fermions. Their presence in the SDW phase of the iron-pnictides was theoretically predicted [14], and suggested to play an important role in transport properties [15, 16]. Moreover, a Dirac cone was observed in the electronic structure of BaFe_2As_2 by angle resolved photoemission spectroscopy (ARPES) [17] and was shown to be consistent with the angle dependence of the magnetic quantum oscillations in BaFe_2As_2 and SrFe_2As_2 [18]. Recent theoretical investigations of Dirac fermions in the parent antiferromagnetic state by Morinari et al. [15] have provided $R_H(T)$, $S(T)$ and $\nu(T)$, whose overall trends agree well with the experimental data presented here (the authors of Ref. [15] used the same "old" sign convention as in Ref. [3]). The authors considered a phenomenological two-band model consisting of a hole band (denoted below with index h) with a conventional energy spectrum, and an electron band (index e) with the Dirac fermion energy spectrum. It is worth emphasizing that even if the Dirac fermions are the minority carriers some transport coefficients exhibit noticeable contributions from Dirac fermions and the Nernst coefficient is expected to be significantly affected [15]. ν was calculated as: $\nu = (\alpha_{xx}\sigma_{xy} - \alpha_{xy}\sigma_{xx})/[B(\sigma_{xx}^2 + \sigma_{xy}^2)]$, the Hall coefficient as: $R_H = \sigma_{xy}/(B\sigma_{xx}^2)$ and the thermopower as: $S = \tau\alpha_{xx}$, where α_{ij} and σ_{ij} are elements of the Peltier and electrical conductivity tensors, respectively, and τ is the relaxation time. Results are the sum of contributions from the two bands. The inset to Fig. 3 shows

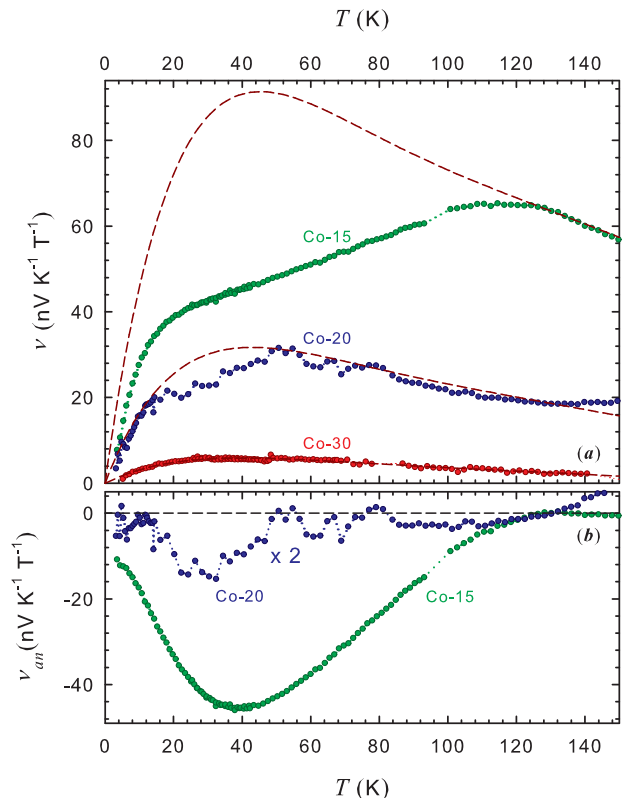


FIG. 4: (Color online) Separation of $\nu(T)$ in Co-15 and Co-20 into the normal (ν_{met}) and anomalous (ν_{an}) components. Panel (a) shows the experimental data (points) and fitted $\nu_{met}(T)$ (dashed lines). Panel (b) presents the estimated $\nu_{an}(T)$ for Co-15 and Co-20 (the latter is multiplied by 2).

the comparison between the theoretical and the experimental data (Co-1), where the latter were multiplied by a constant to match the heights of maxima or minima. The theoretical curves are an exact copy of the results presented by Morinari et al. (Fig. 3(c)) [15] obtained for relaxation times ratio $\tau_h/\tau_e = 0.45$, concentrations ratio $n_e/n_h = 0.05$, and the value of $\varepsilon_0 = \varepsilon_e = k_B T_F$ was taken from Table 2 above. What we would like to stress here is that the response of the electronic system to the onset of SDW is different in Co-0 and Co-15. Furthermore, for the Nernst coefficient this difference is substantial. Namely, in Co-0 there is a sudden rise of ν below T_{SDW} that is very similar to one reported in CaFe_2As_2 [3], while in Co-15 ν for $T < T_{SDW}$ decreases slightly below the high temperature $\nu(T)$ trend. Fig. 4 shows an attempt to separate this anomalous and normal contributions to the Nernst signal. To this end we utilized the purely metallic $\nu_{met}(T)$ dependence of Co-30, which was fitted to the high temperature part of $\nu(T)$ of Co-15 and also Co-20. Fittings were made with two free parameters: $\nu_{met}(T) = aT + b\nu_{Co-30}(T)$, where a and b were supposed to provide for variation of the of the Nernst coefficients due to modification of scattering and concentration of the

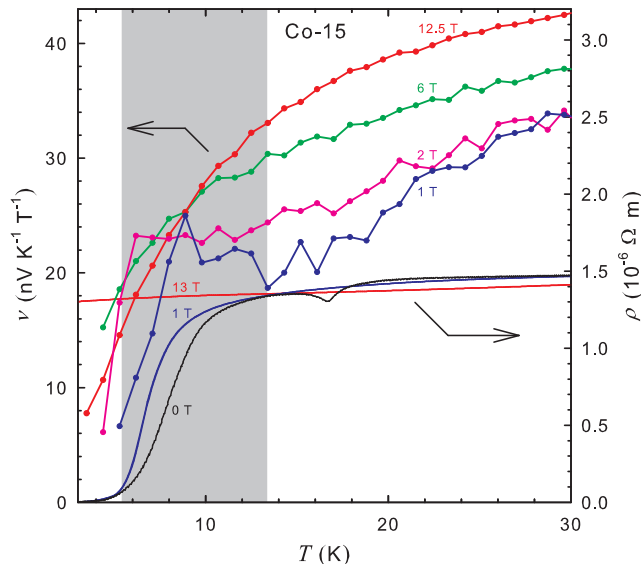


FIG. 5: (Color online) The temperature dependences of the Nernst coefficient (left axis) and resistivity (right axis) for Co-15 measured at various magnetic fields. The shaded area denotes the temperature range, where $\nu(T)$ at $B = 1$ T seems to be influenced by superconducting fluctuations.

charge carriers by Co-doping. The total Nernst coefficient is assumed to simply be a sum of the normal (ν_{met}) and anomalous (ν_{an}) parts: $\nu(T) = \nu_{met}(T) + \nu_{an}(T)$. $\nu_{an}(T)$ obtained in this way for Co-15 and Co-20 are presented in Fig. 4 (b). The onset of the anomaly in Co-15 correlates with T_{SDW} , and is likely associated with the Fermi surface reconstruction caused by spin modulations. A description of the normal-state Nernst signal in the presence of spin-only, charge-only, and combined spin and charge stripe order was recently proposed by Hackl et al. [24]. The authors employed a phenomenological quasiparticle model combined with a Boltzmann equation approach and showed that Fermi pockets caused by translational symmetry breaking can lead to an enhancement of ν . The sign of the anomaly depends on the strength as well as the period of the modulation. Since stripe fluctuations were suggested to be sufficient to cause the Nernst coefficient to increase [25, 26], a small anomaly in $\nu(T)$ that is present in the Co-20 crystal below $T = 50$ K might be attributed to SDW fluctuations. However, a very limited size of this maximum does not allow us to draw definitive conclusions.

While the onset of the SDW order has undoubtedly a significant impact on the electronic transport properties, the local magnetic order in the Eu sublattice seems to have no effect on the Nernst signal. Figure 5 shows the $\nu(T)$ dependences for Co-15 measured at various B . A positive contribution to ν visible at $B = 1$ T and 5 K $< T < 13$ K correlates with the superconducting transition and most probably is a trace of vortex movement. There

is no other anomaly at low fields ($B = 1$ and 2 T), where the influence of the antiferromagnetic Eu^{+2} ordering on the resistivity is still noticeable. A field dependent ν seems to be related to the presence of the SDW order and it is also observed in the non-superconducting Co-0 crystal. We were unable to detect the nonlinearity of $\nu(B)$ in Co-20 and there is no detectable Nernst signal from the SC fluctuations/vortices as in the previously reported case of $\text{Ca}(\text{Fe}_{0.96}\text{Co}_{0.04})_2\text{As}_2$ [3]. In Co-30 the nonlinearities in $\nu(B)$ are absent as well. These results confirm the weak electronic coupling between the Eu and FeAs sublattices [22, 23].

In summary, we have presented data indicating that the low temperature transport properties of the EuFe_2As_2 parent compound are dominated by Dirac fermions thus this compound can be considered as a nodal SDW material. Co doping causes the sudden change of characteristic in the SDW state and the influence of the Dirac fermion vanishes in the superconducting $\text{Eu}(\text{Fe}_{0.85}\text{Co}_{0.15})_2\text{As}_2$. An open question is whether this is a consequence of changes of tiny electron pockets induced by a shift of the Fermi level, or rather increased scattering Dirac fermions, or perhaps an interaction between the nodeless s^\pm type superconductivity and gapless Dirac fermions [27].

Acknowledgments

The authors are grateful to L.J. Spalek, A. Hackl, J.R. Cooper and T. Morinari for useful comments and to M. Malecka for performing the EDX analysis. This work was supported by a grant No. N N202 130739 of the Polish Ministry of Science and Higher Education.

-
- [1] P.A. Lee et al., Rev. Mod. Phys. **78**, 17 (2006), and references therein.
 - [2] S. Sebastian et al., J. Phys. Condens. Matter **20**, 422203 (2008).
 - [3] M. Matusiak et al., Phys. Rev. B **81**, 020510(R) (2010).
 - [4] K. Behnia, J. Phys.: Condens. Matter **21**, 113101 (2009).
 - [5] M. Tegel et al., J. Phys.: Condens. Matter **20** (2008) 452201
 - [6] H.S. Jeevan, et al., Phys. Rev. B **78**, 052502 (2008).
 - [7] S. Jiang et al., Phys. Rev. B **80**, 184514 (2009).
 - [8] J.J. Ying et al., Phys. Rev. B **81**, 052503 (2010).
 - [9] M. Nicklas et al., arXiv:1006.3471v1 (unpublished).
 - [10] Z. Ren et al., Phys. Rev. Lett. **102**, 137002 (2009).
 - [11] H.S. Jeevan et al., arXiv:1011.4481v2 (unpublished).
 - [12] C.F. Miclea et al., Phys. Rev. B **79**, 212509 (2009).
 - [13] E.H. Sondheimer, Proc. R. Soc. London, Ser. A **193**, 484 (1948).
 - [14] Y. Ran et al., Phys. Rev. B **79**, 014505 (2009).
 - [15] T. Morinari et al., Phys. Rev. Lett. **105**, 037203 (2010).
 - [16] K.K. Huynh et al., arXiv:1012.3029v2 (unpublished).
 - [17] P. Richard et al., Phys. Rev. Lett. **104**, 137001 (2010).

- [18] N. Harrison et al., Phys. Rev. B **80**, 224512 (2009).
- [19] Z.A. Xu et al., Nature **406**, 486 (2000).
- [20] I. Kokanović et al., Phys. Rev. Lett. **102**, 187002 (2009).
- [21] Y. Wang et al., Phys. Rev. B **73**, 024510 (2006).
- [22] B. Zhou et al., Phys. Rev. B **81**, 155124 (2010).
- [23] T. Terashima, J. Phys. Soc. Jpn. **79**, 103706 (2010).
- [24] A. Hackl et al., Phys. Rev. B **81**, 045102 (2010).
- [25] O. Cyr-Choiniere et al., Nature **458**, 743 (2009).
- [26] L. Taillefer, J. Phys.: Condens. Matter **21**,164212 (2009).
- [27] M.Z. Hasan et al., Physics **3**, 27 (2010).